

Large-Scale Gas Dynamics in the Adhesion Model: Implications for the Two-Phase Massive Galaxy Formation Scenario

R. Domínguez-Tenreiro^{1*}, J. Oñorbe¹, F. Martínez-Serrano² and A. Serna²

¹*Departamento de Física Teórica, C-XI. Universidad Autónoma de Madrid, Madrid, E-28049, Spain*

²*Departamento de Física y A.C., Universidad Miguel Hernández, Elche, Spain*

Accepted . Received ; in original form

ABSTRACT

We have studied the mass assembly and star formation histories of massive galaxies identified at low redshift z in different cosmological hydrodynamical simulations. To this end, we have carried out a detailed follow-up backwards in time of their constituent mass elements (sampled by particles) of different types. After that, the configurations they depict at progressively higher z were carefully analysed.

The analyses show that these histories share common generic patterns, irrespective of particular circumstances. In any case, however, the results we have found are different depending on the particle type. The most outstanding differences follow.

We have found that by $z \sim 3.5 - 6$, mass elements identified as stellar particles at $z = 0$ exhibit a gaseous cosmic-web-like morphology with scales of ~ 1 physical Mpc, where the densest mass elements have already turned into stars by $z \sim 6$. These settings are in fact the densest pieces of the cosmic web, where no hot particles show up, and dynamically organised as a hierarchy of *flow convergence regions* (FCRs), that is, attraction basins for mass flows. At high z FCRs undergo fast contractive deformations with very low angular momentum, violently shrinking them. Indeed, by $z \sim 1$ most of the gaseous or stellar mass they contain shows up as bound to a massive elliptical-like object at their centers, with typical half mass radii of $r_{\text{star}}^{\text{mass}} \sim 2 - 3$ kpc. After this, a second phase comes about where the mass assembly rate is much slower and characterised by mergers involving angular momentum.

On the other hand, mass elements identified at the diffuse hot coronae surrounding massive galaxies at $z = 0$ do not display a clear web-like morphology at any z . Diffuse gas is heated when FCRs go through contractive deformations. Most of this gas remains hot and with low density throughout the evolution.

To shed light on the physical foundations of the behaviour revealed by our analyses (i.e., a two-phase formation process with different implications for diffuse or shocked mass elements), as well as on their possible observational implications, these patterns have been confronted with some generic properties of singular flows as described by the adhesion model (i.e., potential character of the velocity field, singular versus regular points, dressing, locality when a spectrum of perturbations is implemented). We have found that the common patterns the simulations show can be interpreted as a natural consequence of flow properties that, moreover, could explain different generic observational results on massive galaxies or their samples. We briefly discuss some of them.

Key words: cosmology: theory – cosmology: miscellaneous – hydrodynamics – galaxies: formation – galaxies: high-redshift – galaxies: star formation

1 INTRODUCTION

Among all galaxy families, ellipticals¹ are the simplest and those that show the most precise regularities, sometimes in the form of power-law correlations between some pairs of their observable parameters. The Sloan Digital Sky Survey (York et al. 2000, SDSS) has substantially improved the statistics on elliptical, hereafter E, samples. Analyses of the distributions of their luminosities L , projected effective radii R_e and central line-of-sight velocity dispersions $\sigma_{\text{los},0}$ (Hyde & Bernardi 2009), indicate that they follow Fundamental Plane relations, among other correlations. These correlations are consistent with those previously established in the literature (see references and discussion in Bernardi et al. 2003b,c,d) and are thought to carry fundamental physical information on the processes involved in the assembly of Es.

Recently, spectral indices have been identified (H_β , H_γ , H_δ) that break the age-metallicity degeneracy, allowing for an improved stellar age determination in E galaxies through evolutionary synthesis models (see review in Maraston et al. 2003). Even if still hampered by uncertainties, these models point now to more massive Es having older mean ages and lower rates of recent star formation and, also, higher suprasolar $\alpha/ \langle \text{Fe} \rangle$ ratios than less massive ones. The values of these ratios and their correlation with mass indicators suggest that an important fraction of the stars in most massive galaxies formed on short time-scales, and that this fraction increases with $\sigma_{\text{los},0}$ or galaxy mass. (see Thomas et al. 2005; Gallazzi et al. 2006; Sánchez-Blázquez et al. 2006; Jiménez et al. 2007; Clemens et al. 2009, and references therein). These age effects link elliptical dynamical properties with the characteristics of their stellar populations, and are another manifestation of the physical regularities underlying massive galaxies. Such an effect is also known as the downsizing phenomenon, first introduced by Cowie et al. (1996). Understanding the origin of such regularities in massive galaxy samples is a very important task and it is now affordable.

Two views have historically existed on how elliptical galaxies formed. In the classical *monolithic collapse scenario* (Eggen, Lynden-Bell & Sandage 1962; Tinsley 1972; Larson 1974), ellipticals form at high z in a single burst of star formation ensuing the collapse of a gas cloud. The modern version of the monolithic collapse scenario puts the stress on the assembly out of gaseous material (that is, with dissipation). This assembly can be either in the form of a unique cloud or of many gaseous clumps, but not from pre-existing stars. Indeed, the stellar populations formed at high z and on short time-scales relative to spirals (Matteucci 2003). The competing *hierarchical scenario* (e.g. Toomre 1977; White & Rees 1978) propounds that galaxies form hierarchically through successive random mergers of subunits (the so-called galaxy merger tree) over a wide redshift range, in such a way that more massive ones (that is, ellipticals) are more likely to form at later times. The stress here is on no dissipative assembly through random mergers and on large formation time-scales for the stellar populations.

The regularity of the E family shown by the correlations described above, as well as age effects in massive Es, seem to favour the monolithic collapse scenario. In fact, they are difficult to explain in models where massive galaxies are assembled at late times by

* E-mail: rosa.dominguez@uam.es

¹ Low-redshift galaxies divide into two distinct families at a stellar mass of $\approx 3 \times 10^{10} M_\odot$ (Kauffmann et al. 2003a,b), with more massive galaxies having the characteristics of elliptical galaxies. In this paper the term *elliptical* will most often be used when we refer to observations.

random mergers of pre-existing subunits, as in the *standard hierarchical model* of galaxy formation. The monolithic scenario also explains another set of observational results on E galaxy homogeneity, such as, for example, i), the lack of significant structural and dynamical evolution of lens E galaxies, at least out to $z \sim 1$ (Treu & Koopmans 2004); ii), the lack of any strong structural evolution in the Fundamental Plane relation since $z \sim 3$ (Trujillo et al. 2004; McIntosh et al. 2005); and iii), the confirmed existence of a population of old, relaxed, massive ($M^{\text{star}} > 10^{11} M_{\odot}$) spheroidal galaxies at intermediate z s ($z \sim 1 - 2$, Cimatti et al. 2002, 2004; Stanford et al. 2004), or that of massive objects with old stellar populations earlier on at $z \sim 4 - 5$ (Mobasher et al. 2005; Wiklind et al. 2008; Mobasher & Wiklind 2010).

However, the monolithic scenario does not recover all the currently available observations on Es, either. Important examples are: i), the growth of the total stellar mass bound up in bright red galaxies by a factor of ~ 2 since $z = 1$ (Bell et al. 2004; Conselice, Blackburne & Papovich 2005; Drory et al. 2004; Fontana et al. 2004; Bundy, Ellis & Conselice 2005; Faber et al. 2007), implying that the mass assembly of most Es continues below $z = 1$; ii), the signatures of merging (Le Fèvre et al. 2000; Patton et al. 2002; Kartaltepe et al. 2007; Lin et al. 2008; Lotz et al. 2008; Conselice et al. 2009; Bridge, Carlberg & Sullivan 2010) in particular of major dissipationless mergers between massive galaxies (Bell et al. 2006; Bundy et al. 2009), that translate into a relatively high merger rate even below $z = 1$; and iii), the need for a young stellar component in some E galaxies (van Dokkum & Ellis 2003; van der Wel et al. 2004), or, more particularly, the finding of blue cores, that is, recent star formation at the central regions (see Menanteau et al. 2004, and references therein). These examples suggest that mergers at z s below $\sim 1.5 - 2$ could have played an important role in massive galaxy assembly.

Other sets of observational data that any scenario on massive galaxy formation has to interpret include: i), the existence of a diffuse, X-ray emitting gaseous corona around ellipticals, and the correlations their properties show with those of the galaxy they surround (Beuing et al. 1999; Diehl & Statler 2005); ii), the correlations among black hole properties at the centres of ellipticals and those of their hosting galaxy (Magorrian et al. 1998; Gebhardt et al. 2000; Ferrarese & Merritt 2000; Ferrarese & Ford 2005), as well as the starburst-AGN connection (Aretxaga, Kunth & Mújica 2001); and iii), the relative stability of massive galaxies shapes at low redshifts, while less massive galaxies acquire on average their stable shapes later on (Zheng et al. 2005; Neichel et al. 2008).

In order to reconcile all this observational background within a formation scenario, it is preferable to study galaxy assembly from simple physical principles and in connection with the global cosmological model. Self-consistent gravo-hydrodynamical simulations are a very convenient tool to work this problem out (Navarro & White 1994; Tissera, Lambas & Abadi 1997; Thacker & Couchman 2000). Individual galaxy-like objects including massive ones naturally appear as an output of the simulations, and no prescriptions are needed as far as their mass assembly processes are concerned at scales of a few hundred kpc.

Besides, the results of a self-consistent simulation will be more easily understood in the context of physical theories for the advanced non-linear stages of gravitational instability, just as the results of an experiment can be better understood or interpreted when experimenters have a theoretical background at their disposal. Such a physical theory is provided by the Zeldovich approximation (Zeldovich 1970) and its extension to the adhesion model (Gurbatov & Saichev 1984; Gurbatov et al. 1989; Shandarin & Zeldovich 1989; Gurbatov et al. 1991; Vergassola et al. 1994), including singularity dressing (Domínguez 2000) and gas physics.

The adhesion approximation has already been used in the context of N-body simulations

to predict when and where large scale singularities or caustics (i.e., the skeleton of the large scale mass distribution) form (Kofman, Pogosyan & Shandarin 1990; Weinberg & Gunn 1990). In this case, it showed its potentialities to study a wide class of cosmological problems at these scales. Here we will use it as a theoretical framework to try to understand the mass assembly of massive galaxies as an accretion process onto caustics or "caustic dressing" at smaller scales, including gas processes. Indeed, the aim of this paper is to study hydrodynamic simulations in more detail in this context. More particularly, we analyse the implications that different aspects of the dynamics of singular flows in an expanding Universe (singularity patterns, dressing, locality) could have on the mass assembly processes of massive galaxies. In other words, we aim at deepening the links among some aspects of flow dynamics and different observational characteristics of massive galaxies recently discovered, and that could be a consequence of how these galaxies have acquired their baryons at scales of some few hundred kpc. To avoid that these links get hidden by detailed subresolution modelling, we will remain at the simplest level in this respect.

This paper is organised as follows. The theoretical context is briefly introduced in §2. The simulation method is presented in §3, where we also very briefly outline the comparison of the properties of massive objects formed in the simulations with observational data on ellipticals. In §4 we analyse cosmological hydrodynamical simulations. In §5 we summarise the main results of this paper, we discuss mass assembly within the theoretical background put forward in §2 as well as some of its generic observable implications, and, finally, we give the conclusions of this work.

2 SINGULARITY PATTERNS, DRESSING, LOCALITY

The advanced non-linear stages of gravitational instability are described by the *adhesion model* (Gurbatov & Saichev 1984; Gurbatov, Saichev & Shandarin 1989; Shandarin & Zeldovich 1989; Gurbatov et al. 1991; Vergassola et al. 1994), an extension of Zeldovich's (1970) popular non-linear approximation. In comoving coordinates, Zeldovich's approximation is:

$$x_i(\vec{q}, b(t)) = q_i + b(t)v_i(\vec{q}) \quad (1)$$

where q_i and $x_i, i = 1, 2, 3$ are comoving Lagrangian and Eulerian coordinates of fluid elements or particles sampling them (i.e., initial positions at time t_{in} and positions at later times t), respectively; $b(t)$ is the function of time describing the evolution of the growing density mode in linear gravitational instability and taken to be the time variable in the Zeldovich approximation; and $v_i(\vec{q}) \equiv V_i(\vec{q})/\dot{b}a$, with $V_i(\vec{q})$ the initial peculiar velocity field and $a(t)$ the cosmic scale function.

As it is well known, Zeldovich's solution is not applicable beyond particle crossing, because it predicts that caustics thicken and vanish due to multistreaming soon after their formation. However, N-body simulations of large-scale structure formation indicate that long-lasting pancakes are indeed formed, near which particles stick: multistreaming did not take place. The adhesion model was introduced to incorporate this feature to Zeldovich's approximation.

One way of avoiding multistreaming is to introduce a small diffusion term in Zeldovich's momentum equation, in such a way that it has an effect only when and where particle crossings are about to take place. This can be accomplished by introducing a non-zero viscosity, ν , and then taking the limit $\nu \rightarrow 0$. This is the phenomenological derivation of the adhesion model. Physically motivated derivations can be found in Buchert & Domínguez (1998), Buchert, Domínguez & Pérez-Mercader (1999) and others included in the review by Buchert & Domínguez (2005). As in the Zeldovich approximation, in the adhesion model

motion is potential. Hence, the initial velocity field can be expressed as the gradient of a scalar potential field, $\Phi_0(\vec{q})$, describing the spatial structure of the initial perturbation field. It can be shown that the solutions for the velocity field behave just as those of Burgers' equation (Burgers 1948, 1974) in the limit $\nu \rightarrow 0$, whose analytical solutions are known.

The most significant characteristic of Burgers' equation solutions is that they are discontinuous and hence they unavoidably develop shocks, i.e., locations where at a given time the velocity field becomes discontinuous and certain particles coalesce into long-lasting singularities with different geometries². Mathematically, caustics at time $b(t)$ can be considered as singularities in the so-called *Lagrangian map* that transforms the initial point configuration (i.e., Lagrangian coordinates, \vec{q}) into the point configuration at time $b(t)$ (Eulerian coordinates, $\vec{x}(\vec{q}, b)$). A singularity occurs at time $b(t)$ when a non-zero d -dimensional volume V around point \vec{q} in the initial point configuration is mapped to a d' -dimensional (with d' lower than d) volume around point $\vec{x}(\vec{q}, b)$ in Eulerian space. The mass involved in a given caustic is proportional to the volume V . In a three dimensional space ($d=3$), depending on their dimensionality, caustics can be walls ($d'=2$ or surfaces in the Eulerian \vec{x} space), filaments ($d'=1$), and nodes ($d'=0$).

The adhesion model implies that walls are first formed as denser small surfaces (the so-called pancakes), then they grow until they intersect each other along filaments, that on their turn intersect at nodes. This completes the formation of the cellular structure at a given scale. A further complication is that walls, as two-dimensional systems, usually develop filamentary singularities whose formation follows the same patterns as wall formation in the three-dimensional space, but now with $d = 2$ and $d' = 1$. By the same reason, filaments (either in the full 3D cell structure or within walls) usually fragment and develop nodes where a fraction of their mass ends up. We will call them secondary filaments or nodes to distinguish them from primary filaments (at wall intersection) or primary nodes (at primary filament intersection). Secondary filaments or nodes can be seen in numerical simulations. However, they are not predicted by the adhesion model in three dimensions, but are recovered in two and one-dimensional models, respectively.

At nodes, and more particularly at primary ones, shocked mass piles up. So, at a given scale, walls, filaments and nodes (the cosmic web) are successively formed. Walls and filaments are the paths of shocked particles towards nodes and, at a given scale, they are not long-lasting configurations, but rather vanish as the mass piles up at nodes. This is how the cell structure is erased at given scales. It can be shown (Vergassola et al. 1994) that this behaviour is determined by the structure of the minima of the potential function $-\Phi_0(\vec{q})$ and that asymptotically (i.e., at large b) the behaviour of the system is controlled only by its *deepest minima*. Indeed, cells swallow up some of their neighbouring cells associated with less deep minima of $-\Phi_0(\vec{q})$, involving their constituent elements (i.e., walls, filaments and nodes). This causes contractive flow deformations that erase substructure at cell scales through the coalescence of these elements and their mass piling up into essentially a unique node (i.e., a kind of collapse event). We see that the advanced stages of non-linear gravitational evolution act as a kind of short-scale smoothing process on the cosmic web at scales increasingly larger, while the web is still forming at even larger scales. As time elapses, the structure evolution becomes dominated by larger and larger modes of the density field and finer details are removed by merging and collapse of these modes.

Note that this mass piling up occurs mathematically at *zero relative angular momentum* due to the potential character of the initial velocity field. Moreover, and very significantly for

² Shocks are also called caustics and both names will be used henceforth. Shocks should not be mistaken for shock waves, that is, discontinuities that travel inside fluids heating the subvolume in their path and causing its entropy to increase.

massive galaxy formation, Burgers' equation solutions ensure the existence at any time $b(t)$ of *regular points or mass elements*, as those that have not yet been trapped into a caustic at $b(t)$. Because of that, these regular mass elements are among the least dense in the density distribution. Note, however, that due to the complex structure of the flow, singular (i.e., already trapped into a caustic) and regular (i.e., not yet trapped) mass elements need not be spatially segregated, and in fact, they are mixed ideally at any scale.

One could think that shocked mass would end up mostly within zero volume singularities. Remember, however, that the phenomenological adhesion model tells nothing about the internal density or velocity structure of locations where mass gets adhered. Otherwise, numerical simulations indicate that most mass reaching nodes ends up in virialised structures, where gravitational attraction is balanced by velocity dispersion. How does this come about? Just to have a clue from theory, we recall that in his derivation of a generalised adhesion-like model, Domínguez (2000) finds corrections to the momentum equation of the Zeldovich approximation that regularises (i.e., dresses) its singularities. These then become long-lasting structures where more mass gets stuck, but within non-zero volumes supported by dispersion (see also Gurbatov et al. 1989, for a discussion of these effects in terms of the viscosity phenomenologically introduced in the adhesion model). The analyses of N-body simulations strongly suggest that any kind of flow singularity gets dressed (i.e., not only at pancakes, as it has been analytically proven by Domínguez 2000). Therefore, flow singularities become visible as the places where mass piles up.

Indeed, it is known that in N-body simulations, particles are stopped at and get spatially confined in the neighbourhood of nodes, as they change their macroscopic energy into velocity dispersion. In this way, they give rise to self-gravitating configurations in virial equilibrium (i.e., massive halos). These configurations are characterised by mass, velocity dispersion and size scales M_{vir} , $\sqrt{\langle v^2 \rangle}$ and r_{vir} , respectively, linked by the virial theorem (involving also a shape factor of order unity, see Binney & Tremaine 2008). We note that this *purely mechanical* dissipative mechanism, acting on any kind of gravitating matter, has the same origin as the viscous-like forces in a gas. It has also the same consequences, except that pure gravitating matter cannot lose its energy through radiation or other cooling mechanisms. When gas is added, the energy transfer from ordered to disordered motions includes the transformation of velocity dispersion into internal energy (heating) and pressure, and then energy is lost through cooling, mainly at the densest pieces of the cosmic web. The consequences of these processes cannot be deciphered from theory alone but additionally need gravo-hydrodynamical simulations.

In Cosmology one usually assumes that the field of initial density perturbations is gaussian and with power spectrum given by $P(k) \equiv \langle |\delta_k|^2 \rangle = Ak^n$, where $|\cdot|$ means module and brackets mean statistical average. In this case, the statistical properties of Burgers' equation solution in the $\nu \rightarrow 0$ limit are scale invariant in space and time (b) variables, see details in Vergassola et al. (1994). As a consequence, a length-scale appears in the system, the coalescence length defined by $L_c(t) = (Cb(t))^{2/(n+3)}$ (here C is a normalisation constant such that $\langle (\delta v_l)^2 \rangle = Cl^{-(n+1)}$, where $\delta v_l \equiv \langle |\vec{v}(\vec{x} + \vec{l}) - \vec{v}(\vec{x})| \rangle$). Its physical meaning is as follows: at a given time, $b(t)$, coalescence dominates and substructure is substantially erased at scales $l < L_c(t)$, while the initial situation is expected to have changed only very marginally at larger scales. It is worth noting that $L_c(t)$ is defined based on global average values. Note, however, that those regions R where typically $(\delta v_l)^2 > \langle (\delta v_l)^2 \rangle$ have *local* coalescence lengths at a given time larger than average, $L_c(R, t) > L_c(t)$ (and conversely). Therefore, in these regions evolution proceeds faster (more slowly) than average. Also, scales of a given size l suffer a contractive deformation at different times depending on where they are placed, and

they involve different masses. As we will see below, this *locality* has important consequences to explain some massive galaxy properties.

We now turn to more specific issues related to mass assembly in numerical simulations. In simulations using particles to sample fluid elements, it is very easy to know where the particles that constitute a given object at a low $z = z_{low}$ are initially at $b(t_{in})$. In fact, mathematically this represents the image by the *inverse Lagrangian map* of the set of constituent particles at z_{low} . We will call the configuration they define in the Lagrangian \vec{q} space the *proto-object region* for this object (hereafter, POR). The POR of an object can be visualised through the positions at $b(t_{in})$ of its particles. When we consider an arbitrary z , we will talk about the POR of the object *at* z instead, hereafter $PO(z)$. Again, it can be visualised through the positions at this redshift z of the constituent particles of the object (see §4).

We now introduce a useful concept to describe the mass assembly at high z of an object that is bound at a lower z_{low} : the *caustic or shock tree* for this object. Consider the set of constituent or bound particles of the object at z_{low} . The object caustic tree is defined as the set of caustic formation events involving these particles (walls, filaments, nodes as well as their fusions at different scales and at different times) from $b(t_{in})$ until they become bound to the assembled object. It is a generalisation of the merger tree concept in the Press-Schechter theory, enlarged to take into consideration the richer variety of possibilities here. It represents the development of the PORs of the object at different zs . The object gets assembled through its caustic tree involving the particles that at $b(t_{in})$ constitute its POR, whose transformations by the Lagrangian map/caustic tree can be visualised through the corresponding $PO(z)$ s. We remind that, as noted above, the caustic tree development of a given object is already contained in the structure of the minima of $-\Phi_0(q)$ at the object POR.

The description of gravitational instability we have outlined, based on the adhesive behaviour of matter in a fluctuating density field, can be recasted in the language of gravitational collapse (Padmanabhan 1993) and the Press-Schechter theory (Press & Schechter 1974). In particular, $L_c(t)$ is related to the typical mass $M_c(t)$ of collapsed objects (turnaround) at time t appearing in the theory of non-linear spherical collapse. The main difference lies in the geometry (not necessarily spherical or even three dimensional) of the mass accumulation process, and in the scale invariance properties of the solutions summarised in the coalescence length; these are useful concepts to interpret some massive galaxy properties. Turnaround is seen here as a node formation, that is, in the language of the Lagrangian map, as a *contractive deformation* acting on Lagrangian volumes (see above), and, as already said, the merger tree is now the caustic tree. However, the distinction is important, because of its phenomenological implications on galaxy formation (see for example Jones, van de Weygaert & Aragón-Calvo 2010; Aragón-Calvo, van de Weygaert & Jones 2010), and more particularly in mass assembly at high z , as we will see.

3 METHODS

The quantitative aspects of mass assembly in massive galaxies can only be known through gravo-hydrodynamical simulations, conveniently analysed and visualised.

3.1 Codes and SF Implementation

The simulations analysed here are mainly based on the GALFOBS project³.

³ See at <http://www.deisa.eu/science/deciprojects2007-2008//GALFOBS>

We have used the P-DEVA code. This is an OpenMP AP3M-SPH code specially designed to study galaxy assembly in a cosmological context (Martínez-Serrano 2009). In this code, as well as in its previous sequential version DEVA, particular attention is paid that the conservation laws (energy, entropy, momentum and angular momentum) hold as accurately as possible⁴ (see Serna, Domínguez-Tenreiro, & Sáiz 2003, for details).

Star formation processes have been included through a simple parametrisation (Katz 1992) that transforms locally-collapsing gas at kpc scales, denser than a threshold density, ρ_{thres} , into stars at a rate $d\rho_{\text{star}}/dt = c_*\rho_{\text{gas}}/t_g$. Here t_g is a characteristic time-scale chosen to be equal to the maximum of the local gas-dynamical time, $t_{\text{dyn}} = (4\pi G\rho_{\text{gas}})^{-1/2}$, and the local cooling time; c_* is the average star formation efficiency at kpc scales. This implementation of star formation is equivalent to the Kennicutt-Schmidt law. For details on the SF implementation, see Oñorbe et al (2007). No explicit SF feedback or other discrete energy injection mechanisms have been considered. However, they have implicitly taken into account through the particular values given to the ρ_{thres} and c_* parameters. We have chosen to keep at this simple level of subgrid physics modelling because our aim in this paper is to test how far we can reach relative to massive galaxy formation just from the generic properties of singular flows as introduced in §2.

3.2 Runs

We report here on results of hydrodynamical simulations run in the context of a Λ CDM cosmological model whose parameters, as well as those of the field of primordial density fluctuations (i.e., initial spectrum), have been taken from CMB anisotropy data (Dunkley et al. 2009) with priors⁵. The simulations have been implemented in a periodic box of 80 Mpc comoving side, with a gravitational softening of $\epsilon_g = 2.3$ kpc and a minimum hydrodynamical smoothing length half this value. The mass of dark matter and baryonic particles are 1.5×10^8 and $2.4 \times 10^7 M_\odot$, respectively. This gives 512^3 dark matter and 512^3 baryonic particles in the 80 Mpc side box (main simulation), a size that attains cosmological convergence (Power & Knebe 2006).

When analysing galaxy formation in numerical simulations, it is desirable to be sure that the galaxies the simulation produces are consistent with observations at low z s. Due to the extreme CPU consumption by hydrodynamical forces, this is not yet possible for the main GALFOBS simulation. However, we have been able to reach $z = 0$ for several sub-volumes of this main simulation. To do so, we have run several simulations in which we have just computed the gravitational forces for the full box, and the hydrodynamical forces only in a certain region (sub-boxes of 26 Mpc comoving side) out of the total volume. Care has been taken that these sub-volumes sample different environments. In order to not have problems with the interaction of the different sub-volumes, for our analyses we used the data well inside them, in this case cubes of 20 Mpc comoving side. Five such sub-boxes reached $z = 0$ or $z \approx 0$, (S2100, S2109, S2110, S2114 and S2115) and massive galaxy objects (hereafter MGOs) in there were analysed and found to be consistent with observational data of local ellipticals, see Oñorbe (2009).

To compare the mass assembly and SF patterns of MGOs formed in these simulations with those of MGOs obtained in our previous simulations (Oñorbe et al. 2006; Oñorbe et al 2007), several of those have been also studied, focusing on S8743. We recall that the DEVA

⁴ This in particular implies that a double loop in the neighbour searching algorithm must be used, which considerably increases the CPU time

⁵ http://lambda.gsfc.nasa.gov/product/map/current/params/lcdm_sz_lens_run_wmap5_bao_snall_lyapost.cfm

Table 1. Parameters of the simulations and some MGO parameters. (1): Simulation run; (2): $H_0/100 \text{ km s}^{-1}$; (3): Matter density; (4): Baryon density; (5): Power spectrum normalisation; (6): Density threshold; (7): Star formation efficiency; (8) Number of dark matter and baryonic particles; (9) Smoothing length ($h^{-1} \text{ Mpc}$); (10) Virial radius (kpc) (11) Central velocity dispersion ($\text{km} \times \text{s}^{-1}$) (12) Stellar effective radius (kpc) (13) Stellar mass ($10^{10} M_\odot$).

Simulation	h	Ω_m	Ω_b	σ_8	ρ_{thres}	c_*	$N_{DM} + N_{bar}$	ϵ	r_{vir}	$\sigma_{los,0}^{star}$	$R_{star}^{e,bo}$	M_{bo}^{star}
(1)	(2)	(3)	(4)	(5)	(6)	(7)	(8)	(9)	(10)	(11)	(12)	(13)
S2100	0.694	0.295	0.0476	0.852	4.8×10^{-25}	0.3	see text	0.0015	450	233.64	4.47	29.86
S8743	0.65	0.35	0.06	1.18	6×10^{-25}	0.3	$64^3 + 64^3$	0.0015	532	217.03	6.38	26.40

code was used to run these simulations. Also, the primordial spectrum of fluctuations was implemented in a periodic box of 10 Mpc comoving side sampled by 64^3 dark matter and 64^3 baryonic particles, with the same gravitational softening as in the large box simulation. The initial spectrum normalisation was taken slightly high ($\sigma_8=1.18$) to mimic an active region of the universe.

3.3 Results & Comparisons to Observational Data

Galaxy-like objects of different morphologies (disk-like, elliptical-like, irregulars) have been identified in any kinds of simulations. The analyses of their structural and dynamical properties show that they are consistent with observations of the local universe, both for disk-like (Sáiz et al. 2001; Martínez-Serrano et al. 2009) and elliptical-like objects (Sáiz, Domínguez-Tenreiro & Serna 2004; Domínguez-Tenreiro, Sáiz & Serna 2004; Oñorbe et al. 2006; Oñorbe et al 2007; González-García et al. 2009). For details on the mass and velocity distributions of the different components, and on the parameters characterising them, we refer the reader to these publications.

4 THE PROCESS OF MASSIVE GALAXY ASSEMBLY

These agreements with observations indicate that the assembly patterns of simulated objects could mimic key aspects of real massive galaxy assembly patterns. To deepen into the physics underlying such patterns in a cosmological context, we have analysed in terms of the cosmic web dynamics the sequence of events giving rise to MGO formation in the preceding simulations. Here we give a description of their common characteristics by focusing on two such objects (hereafter MGO #1 and MGO #2), formed in two different simulations (S2100 and S8743), whose characteristics are described in Table 1. Some resulting properties of the two MGOs are also given in this Table.

In Figure 1 we show the projections onto a plane of the positions, at $z = 0$, of the particles within a cube centred at the centre of mass of MGO #1. The cube size in kpc is specified in each of the four windows. From left to right and from top to bottom we show the large-scale dark matter distribution, the dark matter distribution at the scale of the virial radius, the hot gas component ($T > 8 \times 10^4$) and the stellar component. Note in Figure 1 that the hot gas component is much less concentrated than the dark matter component, while the stellar component sets at the very central regions. Note also that cold gas clumps (in green) can be seen spatially mixed with the hot gas.

To illustrate mass assembly and star formation histories from high to low redshift, we visualise the PO(z)s of the two MGOs at four z s. To draw the corresponding plots (Figures 2-6), we have proceeded with different steps: i) Consider MGOs #1 and #2 and their constituent particles of different kinds at $z = 0$ (Figure 1). Choose a particle type at this z : dark matter, stellar, cold or hot gas particles and keep the identity of those whose distance to the MGO centre of mass satisfies $r < r_{lim,i}$. We used $r_{lim,i} = 160$ and 190 kpc for $i = \text{dark}$

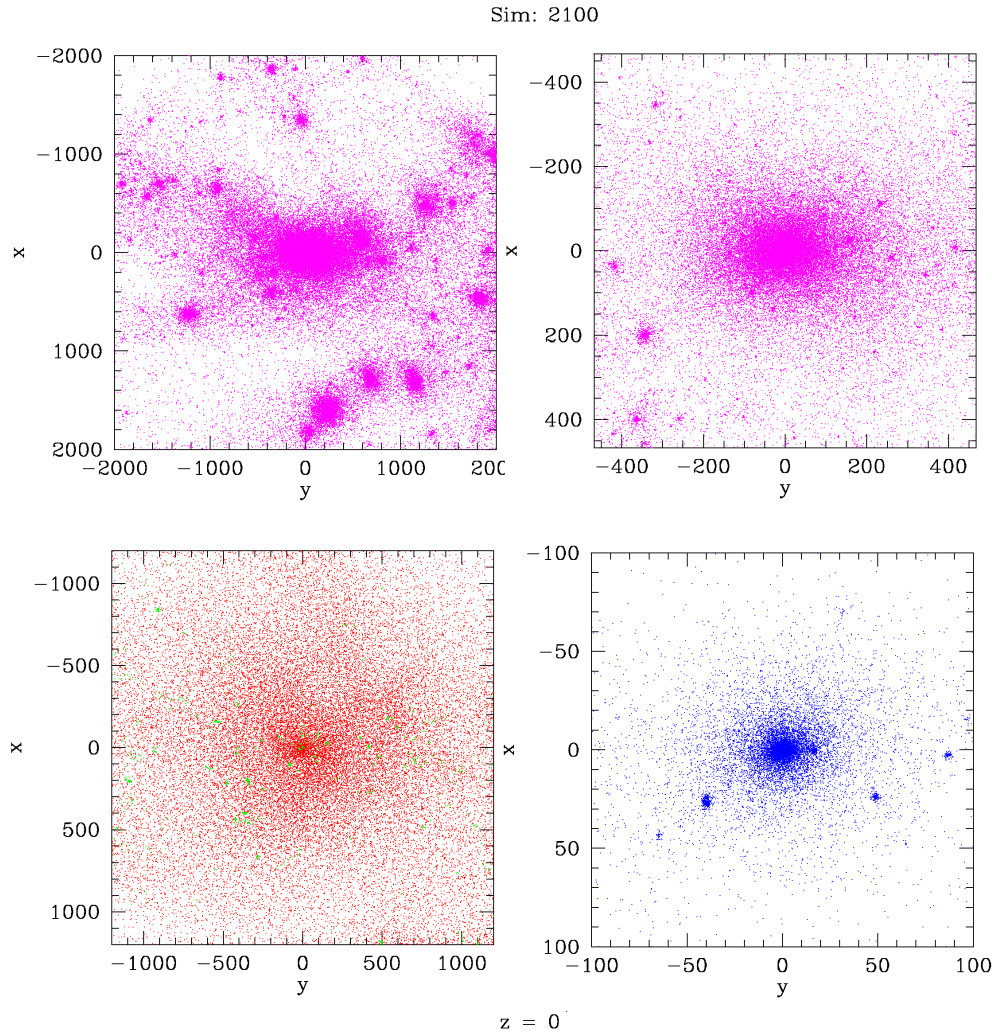


Figure 1. Projections onto the same plane of the positions of particles within cubes centred at the centre of mass of MGO #1 at $z = 0$. From left to right and from top to bottom we show the large-scale dark matter distribution, the dark matter distribution at the scale of the virial radius, the gaseous component (hot gas corona and cold clouds) and the stellar component. Colour codes: dark matter is magenta; hot gas ($T > 8 \times 10^4$) is red; cold gas is green; stellar particles are blue. The window sizes are in kpc.

matter in MGOs #1 and #2, respectively⁶, $r_{\text{lim},i} = 30$ for $i = \text{stellar mass component}$, and $r_{\text{lim},i} = 1200$ and 1500 kpc, for $i = \text{hot gas component}$. ii) Look for the positions of these particles at four different redshifts, $z' = 6.0, 3.5, 2.2$ and 1.0 . Look for the type (either gaseous or stellar) of those particles that at $z = 0$ are stellar particles, as well as the temperature $T(z')$ of those particles that at given z' are gaseous particles. iii) Finally, to draw the Figures in this set, project these positions onto a given plane, the same at any z' , and around the same centre at each z' , using the same colour code as that in Figure 1.

4.1 Hydrodynamic Simulations at Large Scales: an Outline

As other authors', our simulations show that gas roughly follows dark matter at scales larger than a few Mpc. As predicted by the adhesion model and expected from pure gravitational simulations, our simulations indicate that at high redshifts the cosmic web dynamics proceeds as usual. Indeed, evolution causes first the formation of small pancakes that, later on, grow

⁶ these are the radii enclosing half their total mass, including dark matter

and join, forming a three dimensional cellular network, where dense walls and filaments surround underdense regions or voids.

Using three dimensional visualisation techniques, we have seen that matter (dark or baryonic) that first sticks into pancakes moves later on into the filaments, forming a nearly irrotational flow, until it comes to the nodes. Moreover, secondary filaments form into walls, and secondary nodes form within filaments. At pancake, filament and node locations, the velocity field becomes discontinuous and the density field shows very pronounced maxima (caustic locations). These behaviours are illustrated in Figures 2 to 5. Nodes play the role of local attraction basins where mass piles up (this is shocked material in the terminology of the adhesion model). When caustics form, volume contractions are extremely fast and mass becomes trapped, resulting in energy dissipation. At the same time, the gaseous component trapped into singularities begins to be gradually transformed into stars at the densest locations.

This cellular structure is not homogeneous, as the mesh size and the coalescence length $L_c(t)$ depend on position at a given time. And so, some subvolumes enclose denser parts of the cosmic network than others, and are overdense relative to the average box density while other subvolumes are underdense. Their evolution is quite different (*locality* of evolution). In the simulations we see that underdense regions expand for ever. Overdense subvolumes, at a given scale, first expand slower than average. Then their expansion stops, i.e., they turn around, in the language of the spherical collapse scenario. Finally, these subvolumes experience fast global contractive deformations, as the adhesion model indicates (see §2), within collapse time-scales. These fast contractions involve the cellular structure elements the subvolumes enclose, and, in particular, nodes. These nodes are connected by filaments and experience fast head-on fusions as a consequence of subvolume contractions.

We have seen in our simulations that overdense subvolumes at different scales act as *flow convergence regions* (FCRs), i.e. attraction basins for mass flows with defined boundaries in Lagrangian coordinates, whose fate is to shrink following contractive deformations (recall the short-scale smoothing character of the advanced stages of non-linear gravitational evolution). The POR of a given massive object encloses several FCRs, which gradually disappear giving clumps at FCRs of a higher hierarchical level, as visualised and explained in §4.2 below. Each FCR hosts several nodes along with their connecting filaments, where star formation is already on. At the same time, as predicted by Burgers' equation, a certain fraction of gas is never trapped into caustics and it forms a diffuse phase component that fills FCRs unconnected to cold gas. This diffuse gas phase is never involved in star formation and it gets gravitationally heated at violent events.

From a global point of view, we have also seen that from the very beginning different FCRs, corresponding to the PORs of different massive objects, appear in the whole simulation box, and that some of them merge along the evolution. An important point is that FCR properties result from the structure of the minima of the potential function, $-\Phi_0(q)$, that is, they are determined from the very beginning. A consequence is that the amount of mass (either dark or gaseous) available to form an object is fixed ab initio.

4.2 Caustic Tree Development vs Regular Particles

4.2.1 Dark Matter and Star PORs at Different z s

As an illustration of the caustic tree concept, as well as of other ideas introduced in §2, we visualise in Figures 2 and 3 the $PO(z)$ s at four different z s corresponding to the dark matter particles identified at $z_{low} = 0$. In Figures 4 and 5 we visualise the $PO(z)$ s corresponding to the baryonic matter particles that at $z_{low} = 0$ end up as the stellar component of these

two MGOs. As stated above, caustics (the points where singularities build up) stand out in these Figures at $z = 6$ and $z = 3.5$ as the regions where mass piles up, and in fact they are the densest parts of the cosmic web that shows up at these scales. A diffuse component is also evident, and constitutes the regular points at the corresponding z s. Note that this diffuse component tends to flow into caustics, therefore vanishing as evolution proceeds.

We can see in these Figures that at high z the evolution patterns of the dark matter and baryonic components closely follow each other. In fact, at $z = 6$, singularities build up roughly at the same locations in either of these two components. Note also that stars (in blue) are formed from gas located in small clumps at the denser subvolumes of the system, as sampled either by dark matter or baryons. From $z = 6$ to $z = 3.5$, and for either MGO, contractive deformations, acting on different FCRs, bring most baryons into a more marked outstanding filamentary structure. During this process star formation goes on at the densest subvolumes of this filamentary structure. Some of these clumps merge during this period. The dark matter component is also brought by the contractive deformations into more marked filaments. However, a difference with the baryonic component stands out at $z = 3.5$: caustics are thicker in the case of dark matter, which is non-dissipative. Baryons in turn, have dissipative behaviour, and become denser in phase space as they cool.

We now consider the evolutionary patterns of MGO #1 and MGO #2 between $z = 3.5$ and $z = 2.2$. We see that at $z = 2.2$ filaments have practically been removed in favour of clumps, either in the dark matter or the baryonic components (again as a result of contractive deformations). In either MGO #1 or MGO #2, a number of massive clumps stand out at $z = 2.2$. The dark matter halos of these clumps are much more massive and bigger than the baryonic component they host, which is concentrated due to dissipation, and mostly stellar. Note that some of these dark matter halos are about to merge, while their baryonic components are not yet involved in a merging process. In the $z = 2.2$ snapshot, several FCRs can still be seen around the massive clumps, but are now dominated by clumps.

Contraction goes on from $z = 2.2$ to $z = 1.0$. At $z = 1.0$, filaments in both the dark matter and the baryonic components have completely disappeared and dark matter relaxed spheroids have formed (almost relaxed in the case of MGO #1). Note that one such spheroid forms at each FCR seen in the previous snapshot. These dark matter spheroids host most of the baryons that at $z = 0$ form the stellar component of either MGO #1 and MGO #2. Note also that most of these baryons have already been transformed into stars. The stellar component of MGO #1 is involved in a major merger event at $z = 1.0$, resulting in the object depicted in Figure 1. Regarding MGO #2, the four spheroids seen at $z = 1.0$ will eventually merge between $z = 1$ and $z = 0$, resulting in the final object at $z = 0$.

A remarkable fact is that no hot gas particles (in red) show up in these Figures. Otherwise, it is also very remarkable that the assembly patterns for either MGO #1 or #2 are quite similar, both for their dark and stellar components. We remind that S2100 and S8743 have been run with different codes (indeed, the DEVA code has been extensively modified during its OpenMP parallelisation), different box sizes and different values of the cosmological model or the SF parameters. These patterns are common to those we have found for the other massive galaxies in S2100 and S8743, or any other simulation we have analysed.

Note that caustic formation implies different evolution patterns for gas and dark matter at small scales. Otherwise, cooling processes dominate at the densest filaments and nodes, where the gas is cold, while hot gas flows at FCRs end up as a hot corona around the main clumps.

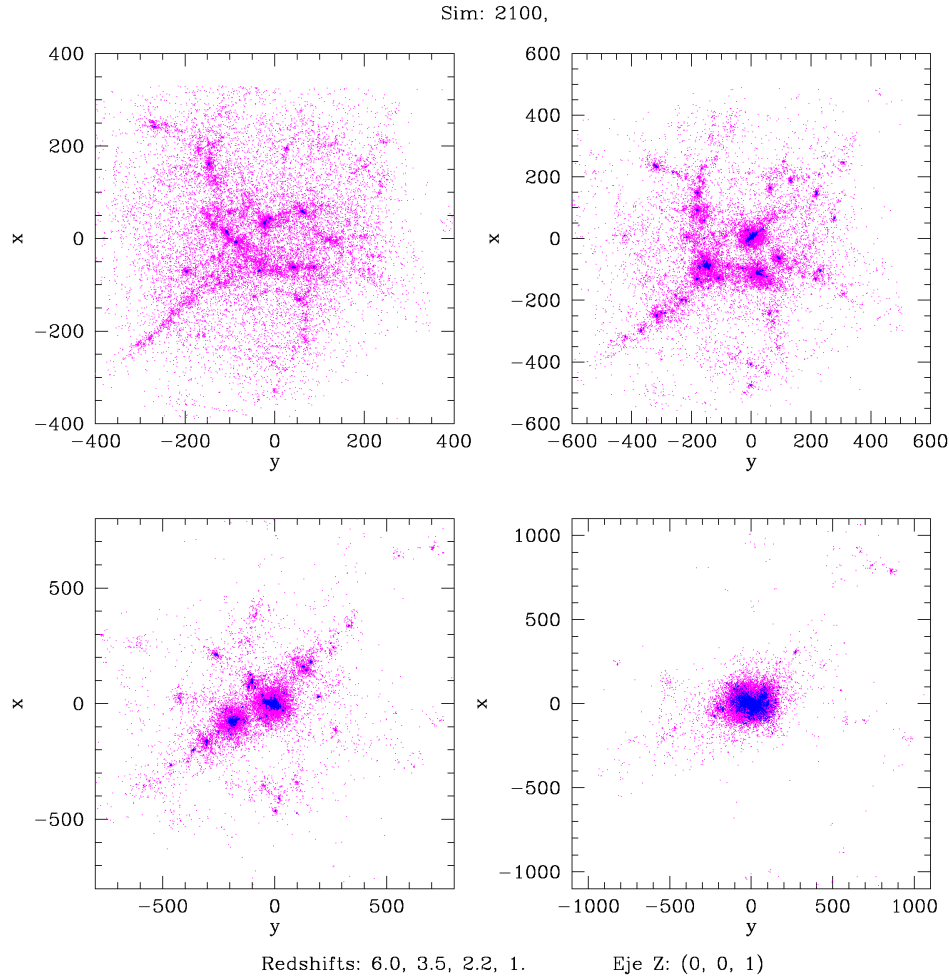


Figure 2. This Figure visualises the $PO(z)$ of MGO #1 at different z s. It shows the projections of the dark matter particles that at $z = 0$ form half the more bounded particles of the halo. From left to right and from top to bottom, the redshifts are $z = 6, 3.5, 2.2$ and 1.0 . Colour code is as in Figure 1. The pieces of the cosmic web displaying different FCRs clearly stand out at high z .

4.2.2 Hot Gas

We now turn to analyse the origin of the hot gas component shown in Figure 1. We focus on the MGO #1 hot gas component, because the patterns for MGO #2 or the other massive galaxies formed in any simulation we have analysed are quite similar. In Figure 6 we show four snapshots, at the same z s than the previous Figures, of those gaseous particles that at $z = 0$ are within $r < r_{\text{lim}} = 1200$ kpc of MGO #1 centre and have temperatures $T > 8 \times 10^4 \text{K}$. In this Figure, green points are cold gas ($T \leq 8 \times 10^4 \text{K}$) while red points are hot gas at the z considered. We can clearly witness in this Figure the gravitational gas heating due to violent dynamical events, that partially transform the mechanical energy involved into contractions into thermal energy. To be quantitative, recall for example that a system must get rid of an amount of energy equal to its binding energy as it collapses from infinity and virialises, see Binney & Tremaine (2008). Hence, gas heating first begins at the densest subvolumes within the system. Another outstanding characteristic is that contractive deformations have quite a different effect on this component than in the dark matter or stellar components. Indeed, even if diffuse gas is pulled by dark matter and tends to move towards the same zones where dark matter does, the total volume they fill at $z = 6$ has not had its shape

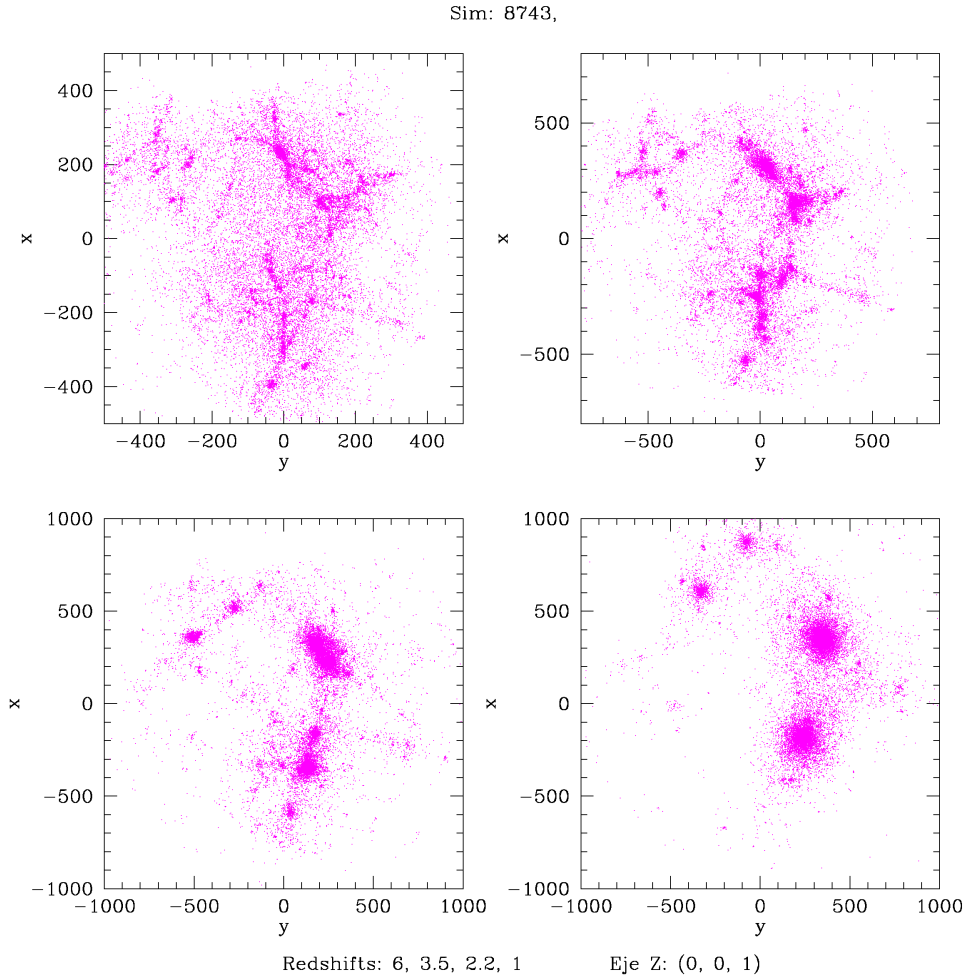


Figure 3. Same as the previous Figure for MGO #2. From left to right and from top to bottom, the redshifts are $z = 6, 3.5, 2.2$ and 1.0 . Different FCRs are clearly apparent as well as their transformations. Between $z = 1$ and $z = 0$, their resulting clumps will merge giving the final object.

significantly deformed between $z = 6$ and $z = 2.2$. In other words, $PO(z)_{hot,gas}$ suffers from less shrinkage and shape changes than $PO(z)_{cold,gas}$ or $PO(z)_{dark,matter}$ (compare Figures 2 and 4 with Figure 6 at $z = 6$ and 3.5). Note that this gas has a much lower phase space density at any z than that of dark matter particles or baryons that eventually end up as the stellar MGO component. Between $z = 3.5$ and $z = 2.2$, diffuse gas follows the collapse of the denser subvolumes of the configuration and heats. From $z = 2.2$ to $z = 1.0$, while the two halos seen in the $z = 2.2$ snapshot complete their merging, gas heats and tends to diffuse due to gas pressure and heating, and mechanical energy conservation. Finally, between $z = 1.0$ and $z = 0$, heating and diffusion keep on acting, until gas forms the hot corona around MGO #1 seen in Figure 1. This behaviour of the hot gas component illustrates the concept of regular mass elements at a given redshift, defined as those that have not yet been trapped into a singularity at this redshift. They are less dense than those that have been trapped. This is the case for the gas in this Figure as compared to the gas providing the mass to form stars (see previous Figures). Remember that the existence of singular and regular mass elements is predicted by Burgers' equation solutions (see §2). In fact, this mathematical distinction between singular and regular mass elements is at the basis of the different physical behaviour we have found between dense gas and diffuse gas

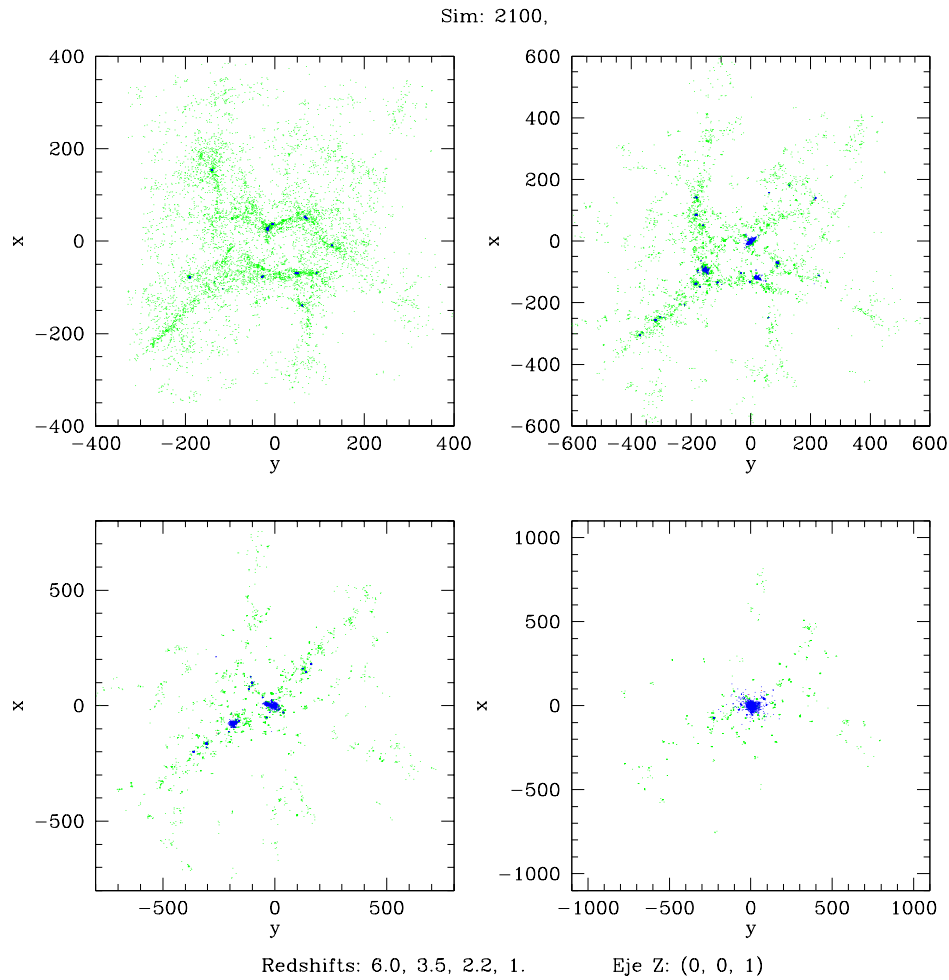


Figure 4. The $PO(z)$ corresponding to the stellar component of MGO #1 at four different z s. This Figure shows the projections of the baryonic particles that at $z = 0$ form the stars of MGO #1. From left to right and from top to bottom, the redshifts are $z = 6, 3.5, 2.2$ and 1.0 . Colour code is as in previous Figures.

in the simulations. Note that a fraction of the gas that transforms into stars is heated as it gets into the object or comes close to it. However, it cools very fast due to its high density (Oñorbe 2009), see also Oñorbe et al. in prep.

4.3 Evolution at the MGO Scale: Star Formation

We now consider the formation and ageing of stars in the same objects as in §4.2. The aim is to assess details of stellar formation as a consequence of dynamical activity and their configuration changes (i.e., irregular shapes, relaxation). To this end, we focus on processes at the scales that are now important (\sim lower than 50 kpc).

We have already seen that at high redshifts, stars first form in the densest and coldest gaseous nodes. As evolution proceeds, flow convergence regions become denser and denser, until they experience global contractive deformations. As seen in Figures 4 and 5, such contractive deformations involve the FCRs of either MGO #1 or #2 from $z \approx 6$ ($t/t_U = 0.068$) to $z \approx 2.2$ ($t/t_U = 0.22$), triggering enormous activity and causing a very fast coalescence of the different FCRs. Indeed, the nodes they host become closer and closer until they hierarchically merge with very low relative angular momentum. This results in very modest orbital delay, which in turn leads to high rates of gas energy dissipation and important

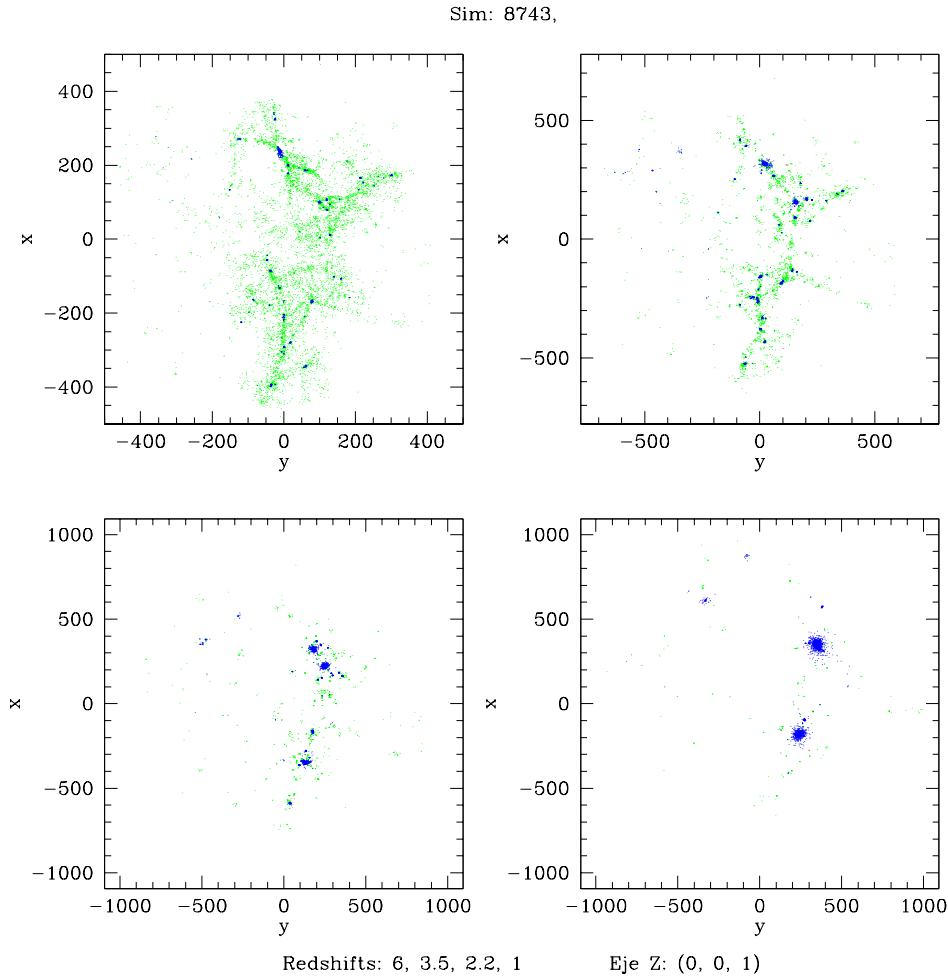


Figure 5. Same as previous Figure for MGO #2. From left to right and from top to bottom, the redshifts are $z = 6, 3.5, 2.2$ and 1.0 . Again, different FCRs and their transformations clearly stand out, as well as the galactic objects they produce by $z = 1$.

bursts of star formation at the nodes. The SFR histories of the stellar population present at $z = 0$ have been plotted in Figures 7 and 8. They indicate that most stars ($\approx 70\%$) were formed when the Universe was younger than 20% of its present age.

By $z \approx 2$ the dynamical activity slows down; the inflow rates decrease and most previously flowing mass is now stuck onto dense small objects (i.e., secondary nodes) that later on fall towards the central object after orbiting it as satellites. Any further MGO mass assembly takes place through merger events with non-negligible relative angular momentum and longer time-scales, involving either small satellites or almost equal-mass objects.

To illustrate this point, the mass aggregation tracks along the main branch of the merger tree have been drawn for the MGOs, for both the baryonic component (mass inside fixed radii) and for its total mass (virial mass) in Figures 7 and 8. These mass aggregation tracks give us information on the mass assembly processes through time. Major mergers ($M_{\text{secondary}}/M_{\text{main}} > 0.25$), minor mergers and slow accretion processes in the dark matter or baryonic component can be clearly identified as discontinuities or slow mass increments, respectively.

The dynamical slowing down of MGO mass assembly at $t/t_U \approx 0.2$ can be clearly appreciated in the mass aggregation tracks (dark matter component), that also causes the MGO baryonic component assembly to slow down. In some cases, the time delay between

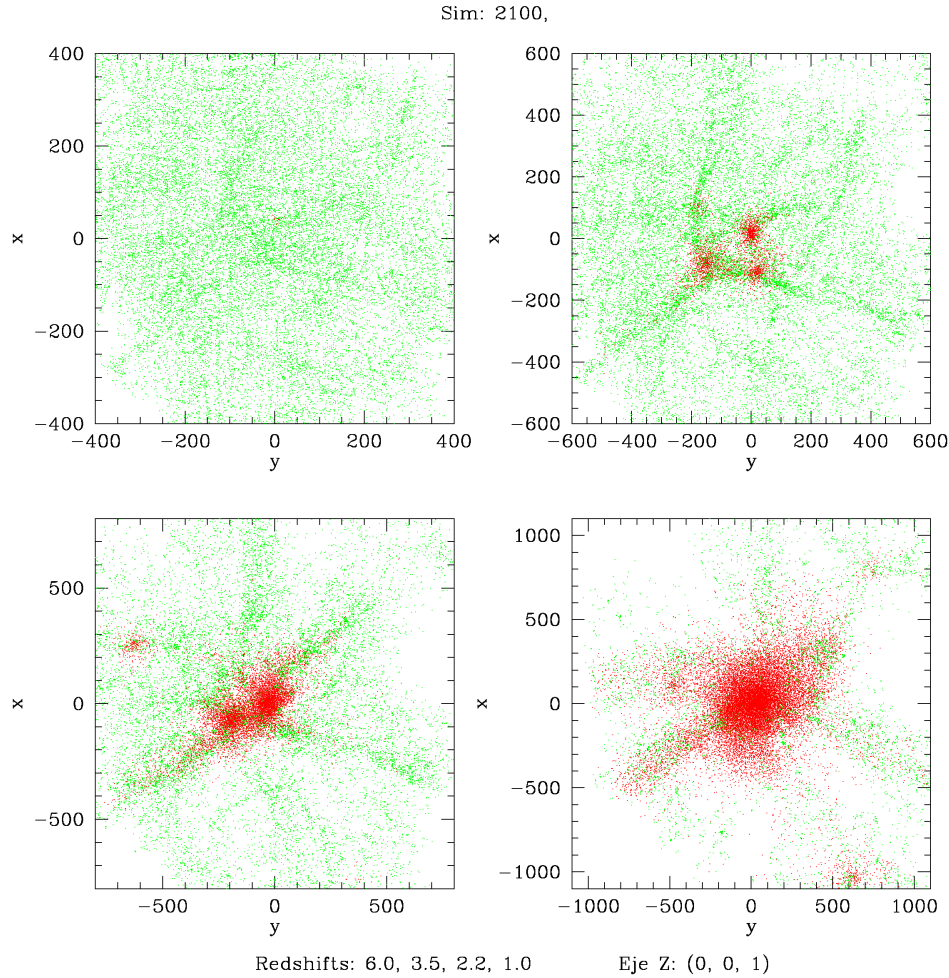


Figure 6. The $PO(z)$ of a massive MGO at four different z s. This Figure shows the projections of the gaseous particles that at $z = 0$ form the hot corona of MGO #1. From left to right and from top to bottom, the redshifts are $z = 6, 3.5, 2.2$ and 1.0 . Colour code is as in previous Figures (red: gaseous particles with $T > 8 \times 10^4 \text{K}$; green: gaseous particles with $T \leq 8 \times 10^4 \text{K}$).

halo and baryonic component coalescence at these lower z s can also be appreciated. This corresponds to an orbiting infall of the merging object around the main.

Stellar objects have irregular shapes while violent dynamical events are ongoing. Afterwards, as the rate of mass assembly slows down, the main object progressively acquires a regular shape, as corresponds to higher and higher degrees of relaxation. A passive ageing of its stellar population can also be appreciated. Gas accretion in this period occurs at a slow rate, while star formation at the centre of the proto-MGO (at a very low but continuous rate) leads to a space segregation of stellar ages.

The first phase of this process, corresponding to the contractive deformation, is termed *fast multiclump collapse*. Some authors have heuristically proposed (Thomas, Greggio & Bender 1999) this concept to account for the need of short SF time-scales at high z in early type galaxies within the hierarchical clustering paradigm. The new point here is that fast multiclump collapse *directly results from the simple physics* involved in our simulations of the evolution of perturbations to a Λ CDM model. In fact, it is a natural and important consequence of the adhesion model we use as a guideline to highlight this underlying physics. The second phase at lower redshift is dominated by classical mergers with a lower rate of mass aggregation.

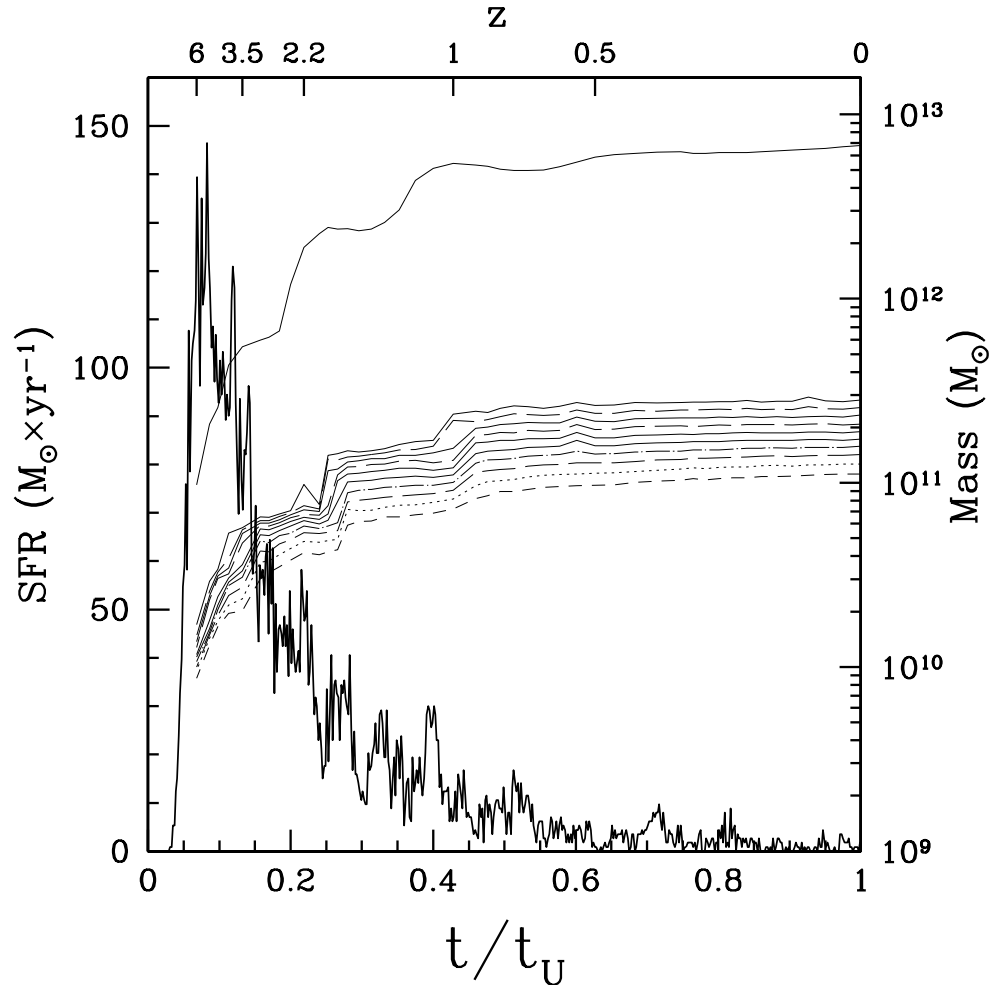


Figure 7. The star formation rate history (solid line) for the same stars drawn in Figure 1 and the mass aggregation track along the main branch of the merger tree for MGO #1. Upper thin full line: the virial mass. Point and dashed lines below: baryonic mass inside different fixed radii, equally spaced in a logarithmic basis from 3 to 30 kpc.

4.4 Two Phase Mass Assembly Process for Massive Galaxies

The mass assembly histories of the particular MGOs outlined in the previous sections are representative of the main patterns present in the general MGO population.

Analytical models, as well as N-body simulations, show that two different phases can be distinguished along *halo* mass assembly (Salvador-Solé, Manrique & Solanes 2005; Wechsler et al. 2002; Zhao et al. 2003): i) first, a violent, fast phase, with high mass aggregation (i.e., merger) rates; and ii) later on, a slow phase, where the mass aggregation rates are much lower. Previous smaller box hydrodynamical simulations had already confirmed this scenario and its implications on MGO properties at low z , see Domínguez-Tenreiro et al. (2006), see also Oser et al. (2010) and Cook, Lapi & Granato (2009). The present analysis, including larger box hydrodynamical simulations, provide information about the consequences of such a scenario on the baryonic component during MGO assembly.

As noted above, during the fast phase at high z , mergers are induced by the collapse of FCRs. They are usually multiple, and involve only low or very low relative orbital momen-

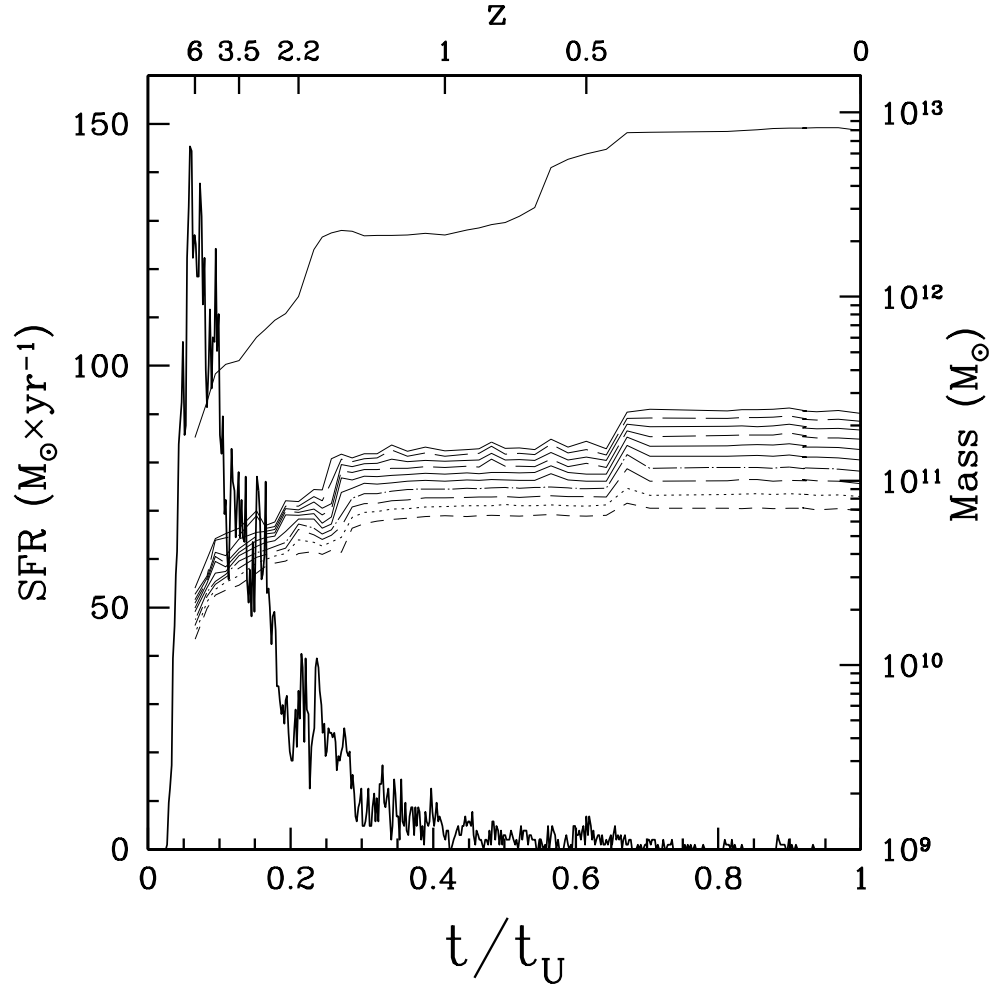


Figure 8. Same as previous Figure for MGO #2.

tum⁷. They are gas rich, so that most of the thermal dissipation occurring along the mass assembly of a given MGO takes place during this phase, and results in strong SF bursts that transform most of the gas available at the FCR at high z into stars.

Later on, during the slow phase, mergers result from coalescence of basins, including the main object and its satellites, as well as the dark matter halo and the diffuse hot gas corona. Mergers now happen with relative orbital momentum so that there is a time delay between the halo fusion and the MGO fusion due to orbital decay. This can be appreciated in Figures 7 and 8 when the aggregation tracks for dark matter and baryons around major mergers are compared, or in the projected images of MGO #1 and #2 at $z = 2.2$. Their rate is much slower, and it can be even zero; that is, some MGO have not experienced any major merger event during this second phase. The actual rate depends on the density of the environment where the MGO lives. Because most gas available at the POR is exhausted during the previous fast phase, the dissipation and SF rates are usually low in this phase, even when a major merger occurs (see Figure 7 at $t/t_U \approx 0.4$, or 8 at $t/t_U \approx 0.65$ where major mergers take place with only very modest consequences on the SFR).

These two phases of mass assembly are responsible for different properties of MGO

⁷ The merger characteristics have been detected and measured using three dimensional visualisation techniques, as well as the mass aggregation trees of the objects (for details see González-García et al. 2009).

samples, see for example Domínguez-Tenreiro et al. (2008). This will be further developed in a forthcoming paper.

5 SUMMARY, DISCUSSION AND CONCLUSIONS

5.1 Summary on Simulation Results Confronted with Singular Flow Properties

The results presented in the previous section help us decipher massive galaxy formation in the light of some generic properties of singular flows, as described by the solutions of Burgers' equation. Our most significant result is that massive galaxies form within *flow convergence regions* (FCRs) as a result of the non-linear evolution of the primordial density fluctuation field. As seen in the simulations, FCRs are overdense regions that act as attraction basins for mass flows and undergo contractive deformations transforming them into nodes of larger scale FCRs (i.e., at a superior level of the hierarchy).

Interpreted within the theoretical framework put forward in §2, our simulations suggest that to form a massive galaxy, three conditions must be met: (i) its caustic tree must include larger shocks than average; (ii) the mass contained in its POR, $PO(z_{in})$, must be of the order of the virial mass of a massive elliptical galaxy; and (iii) its POR must contain very deep minima of $-\Phi_0(q)$ ⁸. We remind that FCR properties, as those of solutions of Burgers' equation, result from the structure of the minima of the potential function, $-\Phi_0(q)$, that is, they are determined from the very beginning. These properties include where massive FCRs of different scales are localised within the simulation box, the Universe age when they collapse, the time-scale for their collapse and the mass they enclose, among others.

According to the time and space scale invariance properties of Burgers' equation, in the absence of energy exchanges (heating and cooling), all caustic trees are similar in a statistical sense, once conveniently rescaled in space and time variables, see §2 and Vergassola et al. (1994). In this case, only one parameter would determine the difference: the mass each caustic tree involves, that is, the mass enclosed by the POR of the object, equal to the sum of the masses of the constituent FCRs. An important point is that mass assembly and star formation can be slowed down by angular momentum. Hence, FCRs where massive galaxies get their mass assembled must be relatively free of vorticity. This condition might not be difficult to be met ab initio in massive FCRs in the adhesion model, where the velocity field is potential. Moreover, as massive FCRs collapse at high z , there might not be enough time for vorticity to build up before their collapse (Buchert & Domínguez 2005; Knebe, Domínguez & Domínguez-Tenreiro 2006; Governato et al. 2004).

As a consequence of the conditions above, in the regions R defined by the $PO(z)$ of massive galaxies, the coalescence length $L_c(R, t)$ grows faster than average. Remember that $L_c(R, t)$ is defined in such a way that coalescence dominates and substructure is substantially erased at scales smaller than it, at time t and within region R (see §2). Hence, within these regions, the caustic tree is travelled through very fast and the collapse at given scales occurs earlier on than average at these scales. Indeed, our simulations show that a lot of caustic formation takes place at R very soon, including mergers of nodes at very low angular momentum, that is, without any significant orbital delay (short time-scales). The mass inside R gets virialised when the caustic formation event or collapse associated with the deepest minima of $-\Phi_0(q)$ at $PO(z_{in})$ takes place at time t_f . Previously, there had been

⁸ Note that this can be considered as a reformulation of what Evrard et al. (1990) propound, and that PORs fulfilling these requirements are more frequent in subregions of the simulation that are overdense from the beginning.

lots of activity involving caustics of different geometries and on smaller space scales. This activity is associated with less deep minima of $-\Phi_0(q)$, and with their evolution through the swallowing up of cells. At t_f the violent shock involves the structures resulting from previous caustic formation events at smaller scales within R .

Ideally, each one of these events takes the mass (including gas) of the volume they involve into a lower dimensional subvolume (remember the definition of flow singularities in terms of the Lagrangian map given in §2). However, simulations indicate that the singularities get indeed dressed. Simulations results show that most particles involved in caustic formation live in much smaller, shrunk, but three-dimensional regions. In any case, the violent event at t_f associated with the deepest minima of $-\Phi_0(q)$ at $PO(z_{in})$ tends to clean the mass around it, and more so when it involves a large volume. Hence, the amount of mass available to be further accreted after t_f is severely limited. This would explain why the mass accretion rate is in many cases drastically reduced afterwards.

Apart from mass involved into singularities, Burgers' equation solutions ensure the existence at any time t of regular points or mass elements, as those that have not yet been trapped into a singularity at t (§2). This is confirmed by the simulations, and allows us to understand the presence of a large-scale diffuse, hot gas component. This component has been gravitationally and hydrodynamically heated in violent events (either collapse or contractive deformations at high z , and major mergers at lower z values) and it carries a fraction of the mechanical macroscopic energy and momentum involved in these events. Remember that to assemble a mass M_{vir} , the system has to get rid of an amount of energy equal to its binding energy, which per unit mass is proportional to $M_{\text{vir}}^{2/3}$. So, even when thermal energy exchanges are allowed for, M_{vir} is a key parameter.

We have presented a global point of view for the process of mass assembly. From the point of view of the massive object that is being assembled, our simulations indicate that, at high z , MGOs get their baryons either through almost equal-mass mergers of subunits made out of gas and stars and connected by filaments, or through smoother gas accretion along filaments. Most accreted gas is cold and dense, and it has been previously involved in caustic (pancake and filament) formation, while at any z a fraction of gas or dark matter has never been involved in this kind of events.

5.2 Some Generic Observable Implications

Some currently available observations on massive ellipticals can be explained in this scenario of *flow convergence regions*. Here we focus on the most generic and physically relevant consequences of this scenario, at a rather qualitative level. We postpone the quantitative discussion of more detailed, observationally related consequences to a future paper.

(i) The existence of regular mass elements (i.e., a diffuse gas component) is assured by Burger's equation. Due to its low density, this diffuse component cannot cool rapidly, and remains as a high-frequency radiation emitter (i.e., X-rays in massive ellipticals or groups). Moreover, most hot particles do not fall towards the centre of the MGO configuration, but their distribution is at the scale of the virial radii or beyond (Oñorbe et al 2007).

(ii) From a global point of view, the evolution of high- z mass density elements (either dark or baryonic) consists in their accumulation within attraction basins around flow singularities (except for regular mass elements). Due to dissipative processes, the tendency to accumulate is even stronger in the case of baryons belonging to caustic trees. In this context, black hole formation at high z at the points of flow convergence (the centres of elliptical galaxies or of spiral bulges) appears quite natural. Their later growth in a scenario of co-

evolution for spheroid and black hole mass accretion, fed by gas inflows from their FCRs, and self-regulated at smaller scales by more complex astrophysical local processes (see for example, Silk & Nuslen 2010, and references therein) could explain many of the correlations black holes and their hosts show. A tantalising interpretation is that black holes at the centres of massive galaxies come from *node-like flow singularities*, while the massive galaxies correspond to their *dressing*.

(iii) We now address the role of M_{vir} to build up correlations. M_{vir} is the halo total mass-scale once the object gets bound, and the mass enclosed at its POR (or $PO(z)$) before this happens. To make its role clear, sometimes it is easier to talk about the mass corresponding to the massive FCRs that end up in the bound object at low z .

We first address correlations involving the stellar mass of the massive galaxies, $M_{\text{bo}}^{\text{star}}$. Stars form at shocks ensuing caustic formation. According to §3.1, the gas mass fraction susceptible to be transformed into stars in a given caustic event is equal to the fraction of gas involved in this event whose density is higher than the threshold density ρ_{thres} . According to the Kennicutt-Schmidt-like law implemented in our simulations, those gaseous elements with densities above the threshold are subsequently converted into stars with a time-scale set by t_g/c_* , where c_* is the star formation efficiency parameter. For massive galaxies, the time-scale must be short so that most gas elements above the density threshold are rapidly transformed into stars. In a FCR, the gaseous mass involved in a caustic event is roughly proportional to that of dark matter. Hence, the stellar mass produced at each caustic event is roughly proportional to the dark matter it involves. Otherwise, the stellar mass of an object at a given redshift $z1$ is the sum of the stars produced in each caustic event of its caustic tree at $z1$. These facts explain the correlation found between the intrinsic parameters M_{vir} and $M_{\text{bo}}^{\text{star}}$, and indicate that the correlations are primarily with M_{vir} for the intrinsic objects, see Oñorbe et al. (2005) and Oñorbe (2009). Moreover, as explained above, the amount of energy a system has to get rid of per unit mass to bound a mass M_{vir} is proportional to $M_{\text{vir}}^{2/3}$. This is in part inverted into dynamical heating, that is, velocity dispersion. This explains the correlation found between M_{vir} and the velocity dispersion at different scales, see Oñorbe et al. (2005).

Now, as $M_{\text{bo}}^{\text{star}}$ is proportional to luminosity L for ellipticals (Kauffmann et al. 2003a,b), we infer that M_{vir} should be correlated with luminosity too. As M_{vir} is also correlated with $\sigma_{\text{los},0}$, we deduce that L and $\sigma_{\text{los},0}$ should be also correlated. This is the Faber-Jackson relation (Faber & Jackson 1976; Bernardi et al. 2003a). Note, however, that there is a third parameter: the size. It depends on M_{vir} through the virial relation, and the tilting of the fundamental plane due to dissipation, see Hyde & Bernardi (2009) and references therein. For details on the results of simulations, see Oñorbe et al. (2005) and Oñorbe (2009).

(iv) Second, we address correlations involving age effects of the stellar populations. Remember that, as we said in §1, observations suggest that the stellar populations of massive galaxies have older mean ages and lower rates of recent star formation than less massive ones, and that these effects increase with their mass. The following considerations help to understand them.

As explained before, the amount of gas transformed into stars at a given time at a given FCR depends on how many caustics have formed within it, and the gaseous mass each of them involves. Thus, the relative amount of gas transformation depends on the dynamical activity at the FCR. As for the dynamical activity, in those $PO(z)$ s defining subregions R with higher mass-scales, M_{vir} , the local coalescence length $L_c(t, R)$ tends to grow faster than average, and the time unit tends to be locally shorter than at other R 's where it grows slower. Hence, statistically the same processes occur at R and at R' , but earlier on, faster

and involving more gaseous mass at R . Consequently, the tendency is that stars form and the available gas becomes exhausted earlier on, and on shorter time-scales, within those PORs whose mass-scale M_{vir} is higher. This *dynamical downsizing* (i.e., earlier cold gas consumption at more massive PORs due to enhanced dynamical activity) is just a consequence of Burgers' equation. Of course, this interpretation does not exclude that other physical or astrophysical processes, acting at smaller scales, come into play and conspire to stop star formation at massive ellipticals, see discussion for example at Pipino, Silk & Matteucci (2009) and references therein.

(v) Massive old objects in a young Universe (at redshift z_{high}) can be explained as the consequence of a global contractive deformation acting on a $PO(z)$ involving much more mass than average, implying that it has already collapsed and most of the available gas there has been transformed into stars at z_{high} . Moreover, if its neighbouring $PO(z)$ s evolve by themselves, then the MGO would have had time to dynamically relax before being disturbed by a violent event. Both are possible situations in our scenario, and in fact we have obtained a number density of such objects at $z = 4$ that is consistent with available data (Oñorbe et al. 2010 to be submitted).

(vi) The formation scenario highlighted by our simulations indicates that the mass infall rate onto a given MGO is very high at the time when its FCR collapses. At that time, the gaseous mass elements either travel up to the very centre, feeding the central black hole, or are transformed into stars. This helps to explain that the SFR history and the AGN luminosity should be correlated, i.e., the more active a galaxy is, the younger and the more massive the host stellar population tends to be, and, moreover, for massive objects both of them peak at high z (Kauffmann et al. 2003c; Falomo et al. 2008).

(vii) Gas in filaments fragments and collapses, forming on their turn nodes. If they are close to a massive proto-object, the nodes and the gas left in the filaments might be captured later on by the attraction basin of the proto-object. In this way, the nodes become satellites, that eventually can merge with the massive object, feeding starbursts depending on how much dense cold gas is available. Central starbursts with this origin could explain blue cores in massive ellipticals, see §1.

(viii) High- z galaxies have in general messy morphologies, with dispersion-dominated kinematics. At lower z s, observations suggest that the later the galaxy type and the later its morphology gets stabilised as z decreases (Zheng et al. 2005; Neichel et al. 2008). This can be explained because the POR mass-scale determines how fast its coalescence length grows on average at PORs of different masses, that is, how fast gaseous mass availability to be accreted is exhausted.

(ix) During the slow phase of mass assembly, merging is still taking place, the stellar mass bound in massive galaxies increases (González-García et al, in prep.), and dry mergers (Conselice et al. 2003) dominate the mass growth (see §1 for observational informations). Thus, the final mass distribution of MGOs, as well as their shapes and kinematical properties, among others, is mostly set by non-dissipative mergers (González-García & van Albada 2003; González-García et al. 2009).

5.3 Discussion and Conclusions

In this paper we present a scenario for massive galaxy formation in a cosmological context evinced from hydrodynamical simulations. The theoretical background follows from an extension of the *adhesion model* to a situation where dressing of flow singularities is taken into account. Gas cooling and heating processes, as well as gas transformation into stars, are also allowed for. Moreover, the locality of flow properties in an inhomogeneous density

field is also considered. This scenario shares characteristics of both the monolithic collapse and hierarchical scenarios, but it is distinct from them both and has implications that could explain generic observational properties of massive galaxies. A two-phase mass assembly clearly shows up in the hydrodynamical simulations analysed in this work.

The scenario summarised in §5.1 requires that gas is transformed into stars very fast at massive FCRs. On the contrary, gaseous structures could be formed, including massive disks, that could survive up to the slow mass assembly phase, and delay massive elliptical formation as a result of mergers of these gaseous systems. An efficient star formation activity demands that short scale gas accumulation is not prevented, for example by angular momentum. So, gas at these massive FCRs must have a low vorticity. This is a condition that might not be difficult to fulfil, at least in some FCRs, because the motion is potential in the adhesion approximation. Thus, very high gas densities at the very short scales where stars are assumed to form (Hennebelle & Chabrier 2010), could easily be attained in an environment of high dynamical activity.

This scenario for massive galaxy formation revealed by the simulations disagrees with the conventional picture of galaxy formation introduced in the classic papers by Rees & Ostriker (1977); White & Rees (1978). According to these influential papers, all the gas in dark matter halos is shock heated to the halo virial temperature. Then hot gas in the denser, inner regions of the halo cools as it radiates its thermal energy (cooling-flow hypothesis, Cowie & Binney 1977; Fabian & Nulsen 1977). The gas finally settles in a centrifugally supported disk, where stars form. Feedback is introduced at this level to avoid that the infalling gas overcools, and to regulate star formation. Later on, mergers of stellar disks would produce spheroidal systems. However, at variance with these expectations, Chandra and XMM observations indicate much less cooling at the centres of both clusters and massive ellipticals than expected (Mathews & Brighenti 2003). There are also some indications that gas that forms galaxies falls in cold and unconnected with the hot gas (Sparks et al. 1989). In consistency with these findings, Binney (2004) argues that virial heated gas cannot cool and give rise to star formation (see also Binney 1977). Instead, stars and galaxies would form out of the significant gas fraction that does not heat at halo virialisation. This is consistent with our results, as well as with those of other SPH simulations (Kay et al. 2000; Fardal et al. 2001; Katz et al. 2003; Kereš et al. 2009). In this scenario, star formation would be regulated by dying star ejections and central black hole heating, which in most massive halos ablate and absorb the infalling cold phase. These feedback mechanisms have not been explicitly taken into account in the simulations we present here, but they are unlikely to suppress cold gas infall through filaments *towards* the centres of the attraction basins of proto-MGOs at high z , because this has to do with a singularity formation. They can, and very likely they do, determine the amount of gas infall *inside* the halos or centres of attraction basins at high z and regulate star formation processes at smaller scales (Slyz et al. 2005). This is mimicked in a sense by the star formation parametrisation we use in this paper. Note, however that the feedback mechanisms or even their direction are still not well known. Indeed, some authors propound an enhancement of the star formation efficiency due to AGN feedback, implying suprasolar $\alpha/ \langle \text{Fe} \rangle$ in massive galaxies (Pipino, Silk & Matteucci 2009), while others find that AGN activity could have the opposite effect (Kawata & Gibson 2005).

To sum up, gravo-hydrodynamical simulations have allowed us to advance our understanding of massive galaxy formation in connection with the global cosmological model, and more particularly of how baryonic matter exchanges at different important scales came about. The simulations are a virtual experiment that mimic galaxy formation and evolution, in such a way that they allow us to deepen into the physical processes causing them. In this paper, we report on MGO mass assembly and stellar formation processes in a series of

simulations that follow what could be expected from the adhesion and singularity dressing models, when gas processes are allowed for. Moreover, direct implications of these models nicely explain different generic properties of elliptical galaxies and their samples, some of which could seem paradoxical within a hierarchical scenario.

Let us stress that the assembly patterns we found here are just a consequence of the advanced non-linear stage of gravitational instability evolution, as described by the *adhesion* model within a Λ CDM cosmological model. Otherwise, they result from simple physical laws acting on quite general initial conditions. This is an important result and, in a sense, it represents a test of the *concordance cosmological model* on the scales relevant to galaxy formation (a few hundred kpc).

ACKNOWLEDGMENTS

The authors are grateful to the anonymous referee for his/her help to improve this paper. We thankfully acknowledge to J. Naranjo and D. Vicente for the assistance and technical expertise provided at the Barcelona Supercomputing Centre, as well as the computer resources provided by BSC/RES (Spain). RDT is happy to thank L.J. Roy for the very motivating discussions on singular flows at the beginning of this work. We thank DEISA Extreme Computing Initiative (DECI) for the CPU time allowed to GALFOBS project. The Centro de Computación Científica (UAM, Spain) has also provided computing facilities. This work was partially supported by the DGES (Spain) through the grants AYA2009-12792-C03-02 and AYA2009-12792-C03-03 from the PNAyA, as well as by the regional Madrid V PRICIT program through the ASTROMADRID network (CAM S2009/ESP-1496). JO was supported by the "Supercomputación y e-Ciencia" Consolider-Ingenio CSD2007-0050 project.

REFERENCES

- Aragón-Calvo M.A., van de Weygaert R., Jones B.J.T., 2010, preprint (astro-ph/1007.0742)
- Aretxaga I., Kunth D., Mújica, R., 2001, eds, Advanced Lectures on the Starburst-AGN Connection, World Scientific
- Ascasibar Y., Yepes G., Müller V., Gottlöber S., 2003, MNRAS, 346, 731
- Bell E.F. et al., 2004, ApJ, 608, 752
- Bell E.F. et al., 2006, ApJ, 640, 241
- Bernardi M. et al., 2003a, AJ, 125, 1817
- Bernardi M. et al., 2003b, AJ, 125, 1849
- Bernardi M. et al., 2003c, AJ, 125, 1866
- Bernardi M. et al., 2003d, AJ, 125, 1882
- Beuing J., Dobereiner S., Bohringer H., Bender R., 1999, MNRAS, 302, 209
- Binney J., 1977, ApJ, 215, 483
- Binney J., Tremaine S., 2008, Princeton, NJ, Princeton University Press, 2008, 361 p.,
- Binney J., 2004, MNRAS, 347, 1093
- Bridge C.R., Carlberg, R.G., Sullivan M., 2010, ApJ, 709, 1067
- Buchert T., Domínguez A., 1998, A&A, 335, 395
- Buchert T., Domínguez A., 2005, A&A, 438, 443
- Buchert T., Domínguez A., Pérez-Mercader J., 1999, A&A, 349, 343
- Bundy K., Ellis R.S., Conselice C.J., 2005, ApJ, 625, 621
- Bundy K., Fukugita M., Ellis R.S., Targett T.A., Belli S., Kodama T., 2009, ApJ, 697, 1369

- Burgers J.M., 1948, Proc. Konink. Nederl. Akad. Wetensch. **1**, 171–199
- Burgers J.M., 1974, Reidel, Dordrecht
- Caldwell N., Rose J.A., Concannon K.D., 2003, AJ, **125**, 2891
- Cimatti A. et al., 2002, A&A, **381**, L68
- Cimatti A. et al., 2004, Nature, **430**, 184
- Clemens M. S., Bressan A., Nikolic B., Rampazzo, R., 2009, MNRAS, **392**, L35
- Conselice C.J., Blackburne J.A., Papovich, C., 2005, ApJ, **620**, 564
- Conselice C. J., Bershadly M. A., Dickinson M., Papovich C., 2003, AJ, **126**, 1183
- Conselice C. J., Yang C., Bluck A. F. L., 2009, MNRAS, **394**, 1956
- Cook M., Lapi A., Granato G. L., 2009, MNRAS, **397**, 534
- Cowie L. L., Binney J., 1977, ApJ, **215**, 723
- Cowie L. L., Songaila A., Hu E. M., Cohen J. G., 1996, AJ, **112**, 839
- Diehl S., Statler T.S., 2005, ApJ, **633L**, 21
- Domínguez A., 2000, Phys. Rev. D, **62**, 103501
- Domínguez-Tenreiro R., Sáiz A., Serna A., 2004, ApJ, **611L**, 5
- Domínguez-Tenreiro R., Oñorbe J., Sáiz A., Artal H., Serna, A., 2006, ApJ, **636L**, 77
- Domínguez-Tenreiro R., Oñorbe J., Serna A., González-García A. C., 2008, ASPC, **390**, 468
- Drory N., Bender R., Feulner G., Hopp U., Maraston C., Snigula J., Hill G.J., 2004, ApJ, **608**, 742
- Dunkley J. et al., 2009, ApJS, **180**, 306
- Eggen O. J., Lynden-Bell D., Sandage A. R., 1962, ApJ, **136**, 748
- Evrard A. E., Silk J., Szalay A. S., 1990, ApJ, **365**, 13
- Faber S. M., Jackson R. E., 1976, ApJ, **204**, 668
- Faber S. M. et al., 2007, ApJ, **665**, 265
- Fabian A. C., Nulsen P. E. J., 1977, MNRAS, **180**, 479
- Falomo R., Traves A., Kotilainen J., Scarpa R., 2008, ApJ, **673**, 694
- Fardal M. A., Katz N., Gardner J. P., Hernquist L., Weinberg D. H., Davé R., 2001, ApJ, **562**, 605
- Ferrarese L., Merritt D., 2000, ApJ, **539L**, 9
- Ferrarese L., Ford H., 2005, Space Science Reviews, **116**, 523
- Fontana A. et al., 2004, A&A, **424**, 23
- Gallazzi A., Charlot S., Brinchmann J., White S. D. M., 2006, MNRAS, **370**, 1106
- Gebhardt, K. et al., 2000, ApJ, **539L**, 13
- González-García A.C., van Albada T.S., 2003, MNRAS, **342**, 36
- González-García A. C., Oñorbe J., Domínguez-Tenreiro R., Gómez-Flechoso M. Á., 2009, A&A, **497**, 35
- Governato F. et al., 2004, ApJ, **607**, 688
- Gurbatov S. N., Saichev A. I., 1984, Radiofizika, **27**, 456
- Gurbatov S. N., Saichev A. I., Shandarin S. F., 1989, MNRAS, **236**, 385
- Gurbatov S.N., Malakhov A., Saichev A.I., 1991, "Nonlinear Random Waves and Turbulence in Nondispersive Media", Manchester University Press, Manchester
- Hennebelle P., Chabrier G., 2009, ApJ, **702**, 1428
- Hyde J. B., Bernardi M., 2009, MNRAS, **396**, 1171
- Jiménez R., Bernardi M., Haiman Z., Panter B., Heavens A. F., 2007, ApJ, **669**, 947
- Jones B.J.T., van de Weygaert R., Aragón-Calvo M.A., 2010, preprint (astro-ph/1001.4479)
- Jorgensen I., 1997, MNRAS, **288**, 161
- Kartalpepe J. S. et al., 2007, ApJS, **172**, 320
- Katz N., 1992, ApJ, **391**, 502

- Katz N., Kereš D., Dave R., Weinberg, D. H., 2003, *The IGM/Galaxy Connection. The Distribution of Baryons at $z=0$* , 281, 185
- Kauffmann G., Colberg J. M., Diaferio A., White S. D. M., 1999, *MNRAS*, 303, 188
- Kauffmann G. et al., 2003a, *MNRAS*, 341, 33
- Kauffmann G. et al., 2003b, *MNRAS*, 341, 54
- Kauffmann G. et al., 2003c, *MNRAS*, 346, 1055
- Kay S. T., Pearce F. R., Jenkins A., Frenk C. S., White S. D. M., Thomas P. A., Couchman H. M. P., 2000, *MNRAS*, 316, 374
- Kawata D., Gibson B., 2005, *ApJ*, 358L, 16
- Kereš D., Katz N., Fardal M., Davé R., Weinberg D. H., 2009, *MNRAS*, 395, 160
- Knebe A., Domínguez A., & Domínguez-Tenreiro R., 2006, *MNRAS*, 371, 1959
- Kofman L., Pogosyan D., Shandarin S., 1990, *MNRAS*, 242, 200
- Larson R. B., 1974, *MNRAS*, 166, 585
- Le Fèvre O. et al., 2000, *MNRAS*, 311, 565
- Lin L. et al., 2008, *ApJL*, 681, 232L
- Lotz J. et al., 2008, *ApJL*, 672, 177L
- Magorrian J. et al., 1998, *AJ*, 115, 2285
- Maraston C., Greggio L., Renzini A., Ortolani S., Saglia R. P., Puzia T. H., Kissler-Patig M., 2003, *A&A*, 400, 823
- Martínez-Serrano F. J., 2009, PhD thesis, Universidad Autónoma de Madrid, http://symmetry.ft.uam.es/fran/PhD_Francisco_Martinez.pdf
- Martínez-Serrano F. J., Serna A., Doménech-Moral M., Domínguez-Tenreiro R., 2009, *ApJ*, 705L, 133
- Mathews W. G., Brighenti F., 2003, *ARA&A*, 41, 191
- Mathis H., Lemson G., Springel V., Kauffmann G., White S. D. M., Eldar A., Dekel, A., 2002, *MNRAS*, 333, 739
- Matteucci F., 2003, *Ap&SS*, 284, 539
- McIntosh D.H. et al., 2005, *ApJ*, 632, 191
- Menanteau F. et al., 2004, *ApJ*, 612, 202
- Mobasher B. et al., 2005, *ApJ*, 635, 832
- Mobasher B., Wiklind T., 2010, in *The Impact of HST on European Astronomy, Astrophysics and Space Science Proceedings*, F. Duccio Macchetto ed., Springer, Netherlands
- Navarro J.F., White S.D.M., 1994, *MNRAS*, 267, 401
- Neichel B. et al., 2008, *A&A*, 484, 159
- Oñorbe J., 2009, PhD thesis, Universidad Autónoma de Madrid, <http://symmetry.ft.uam.es/onorbe/doc/thesis-jonorbe.pdf>
- Oñorbe J., Domínguez-Tenreiro R., Sáiz A., Serna A., Artal, H., 2005, *ApJ*, 632L, 570
- Oñorbe J., Domínguez-Tenreiro R., Sáiz A., Artal H., Serna A., 2006, *MNRAS*, 373, 503
- Oñorbe, J., Domínguez-Tenreiro R., Sáiz A., Serna A., 2007, *MNRAS*, 376, 39
- Oser L., Ostriker J.P., Naab T., Johansson P.H., Burkert, A., 2010, preprint (astro-ph/1010.1381)
- Padmanabhan T., 1993, in *Structure Formation in the Universe*, Ch. 8, Cambridge University Press
- Pagel B.E.J., 2001, *PASP*, 113, 137
- Patton D.R et al., 2002, *ApJ*, 565, 208
- Pipino A., Silk J., Matteucci F., 2009, *MNRAS*, 392, 475
- Power C., Knebe A., 2006, *MNRAS*, 370, 691
- Press W. H., Schechter P., 1974, *ApJ*, 187, 425
- Rees M. J., Ostriker J. P. 1977, *MNRAS*, 179, 541

- Sáiz A., Domínguez-Tenreiro R., Tissera P. B., Courteau S., 2001, MNRAS, 325, 119
Sáiz A., Domínguez-Tenreiro R., Serna A., 2004, ApJ, 601L, 131
Salvador-Solé, E., Manrique, A., Solanes, J.M., 2005, MNRAS, 358, 901
Sánchez-Blázquez, P., Gorgas, J., Cardiel, N., González, J., 2006, A&A, 457, 787
Serna A., Domínguez-Tenreiro R., Sáiz, A., 2003, ApJ, 597, 878
Shandarin S. F., Zeldovich Y. B., 1989, Reviews of Modern Physics, 61, 185
Silk J., Nulsen A., 2010, preprint (astro-ph/1004.0857)
Slyz A. D., Devriendt J. E. G., Bryan G., Silk J., 2005, MNRAS, 356, 737
Sparks W. B., Macchetto F., Golombek D., 1989, ApJ, 345, 153
Stanford, S.A., et al., 2004, AJ, 127, 131
Thacker R.J., Couchman, H.M.P., 2000, ApJ, 545, 728
Thomas D., Greggio L., Bender R., 1999, MNRAS, 302, 537
Thomas D., Maraston C., Bender R., Mendes de Oliveira, C., 2005, ApJ, 621, 673
Tinsley B. M., 1972, ApJ, 178, 319
Tissera P.B., Lambas D.G., Abadi M.C., 1997, MNRAS, 286, 384
Toomre A., 1977, in *The Evolution of Galaxies and Stellar Populations*, eds. B. Tinsley & R. Larson (New Have, CN: Yale Univ. Press)
Treu T., Koopmans, L.V.E., 2004, ApJ, 611, 739
Trujillo I. et al., 2004, ApJ, 604, 621
van der Wel A., Franx M., van Dokkum P.G., Rix H.-V., 2004, ApJ, 601L, L5
van Dokkum P.G., Ellis R.S., 2003, ApJ, 592, L53
Vergassola M., Dubrulle B., Frisch U., Noullez, A., 1994, A&A, 289, 325
Wechsler R.H., Bullock J.S., Primack J.R., Kravtsov A.V., Dekel A., 2002, ApJ, 568, 52
Weinberg D. H., Gunn J. E., 1990, MNRAS, 247, 260
Weiss A., Peletier R.F., Matteucci, F., 1995, A&A, 296, 73
White S. D. M., Rees M. J., 1978, MNRAS, 183, 341
Wiklind T., Dickinson M., Ferguson H. C., Giavalisco M., Mobasher B., Gorgin N. A., Panagia N., 2008, ApJ, 676, 781
York D. G. et al., 2000, AJ, 120, 1579
Zeldovich Y. B., 1970, A&A, 5, 84
Zhao D.H., Mo H.J., Jing Y.P., Borner G., 2003, MNRAS, 339, 12
Zheng X. et al., 2005, A&A, 435, 507